Mon. Not. R. Astron. Soc. **000**, 000–000 (0000) Printed 6 June 2011 (MN LATEX style file v2.2)

The angular momentum of baryons and dark matter halos revisited

Taysun Kimm[1⋆], Julien Devriendt[1,2], Adrianne Slyz[1], Christophe Pichon[3,1,2], Susan A. Kassin[4]†, and Yohan Dubois[1]

[1] *Department of Physics, Denys Wilkinson Building, Keble Road, Oxford, OX1 3RH, United Kingdom*
[2] *CRAL, Université Claude Bernard Lyon I, CNRS UMR 5574, ENS-Lyon, 9 Avenue Charles André, F-69561 Saint-Genis Laval, France*
[3] *Institut d'Astrophysique de Paris, Université Pierre et Marie Curie Paris 6, CNRS, UMR 7095, F-75014, Paris, France*
[4] *Astrophysics Science Division, Goddard Space Flight Center, Code 665, Greenbelt, MD 20771, USA*

6 June 2011

ABSTRACT

Recent theoretical studies have shown that galaxies at high redshift are fed by cold, dense gas filaments, suggesting angular momentum transport by gas differs from that by dark matter. Revisiting this issue using high-resolution cosmological hydrodynamics simulations with adaptive mesh refinement (AMR), we find that at the time of accretion, gas and dark matter do carry a similar amount of specific angular momentum, but that it is systematically higher than that of the dark matter halo as a whole. At high redshift, freshly accreted gas rapidly streams into the central region of the halo, directly depositing this large amount of angular momentum within a sphere of radius $r = 0.1R_{\rm vir}$. In contrast, dark matter particles pass through the central region unscathed, and a fraction of them ends up populating the outer regions of the halo ($r/R_{\rm vir} > 0.1$), redistributing angular momentum in the process. As a result, large-scale motions of the cosmic web have to be considered as the origin of gas angular momentum rather than its virialised dark matter halo host. This generic result holds for halos of all masses at all redshifts, as radiative cooling ensures that a significant fraction of baryons remain trapped at the centre of the halos. Despite this injection of angular momentum enriched gas, we predict an amount for stellar discs which is in fair agreement with observations at z=0. This arises because the total specific angular momentum of the baryons (gas and stars) remains close to that of dark matter halos. Indeed, our simulations indicate that any differential loss of angular momentum amplitude between the two components is minor even though dark matter halos continuously lose between half and two-thirds of their specific angular momentum *modulus* as they evolve. In light of our results, a substantial revision of the standard theory of disc formation seems to be required. We propose a new scenario where gas efficiently carries the angular momentum generated by large-scale structure motions deep inside dark matter halos, redistributing it only in the vicinity of the disc.

Key words: galaxies: formation – galaxies: high-redshift – galaxies: spiral – galaxies: kinematics and dynamics – galaxies: fundamental parameters – cosmology: theory

1 INTRODUCTION

Along with mass, angular momentum growth shapes the fundamental properties of galaxies. Using linear theory, one can show that density perturbations acquire angular momentum through their asymmetric interactions with the larger scale tidal field (Peebles 1969; Doroshkevich 1970; White 1984). Thus one expects the angular momentum of the Lagrangian region encompassing a future virialized structure to scale like $a^2(t)\dot{D}(t)$ until it decouples from the Hubble expansion, where a and $\dot{D}$ are the scale factor of the universe and the linear growth rate of density perturbations respectively (White 1984). Further assuming that the gas experiences the same tidal field as the dark matter, they should initially share their specific angular momentum. Provided this specific angular momentum is conserved as the gas radiatively cools, early studies were able to reasonably match crucial observed relations, such as the Tully-Fisher relation or the size-rotation velocity relation (Fall & Efstathiou 1980; Dalcanton et al. 1997; Mo et al. 1998). In spite of several severe shortcomings in the theory pointed out by authors like Hoffman (1986) (including no account of secondary infall and mergers between virialized objects), this success encouraged all (semi-analytic) galaxy formation models published to date (e.g. Cole et al. 2000; Hatton et al.

⋆ e-mail: taysun.kimm@astro.ox.ac.uk
† NASA Postdoctoral Program Fellow

2003; Croton et al. 2006; Monaco et al. 2007; Somerville et al. 2008; Dutton & van den Bosch 2009; Khochfar & Silk 2011) to rely on the core assumption that gas and dark matter contained within the same virialized structure split specific angular momentum equally. However, the recent findings that the vast majority of galaxies are mainly fed gas by cold, thin and dense filaments which penetrate deep inside the virial radius of their host dark matter halo (e.g. Kereš et al. 2005; Ocvirk et al. 2008; Dekel et al. 2009; Powell et al. 2011) begs for a reassessment of the validity of the classical angular momentum scenario.

According to the standard picture of galaxy formation, gas is first shock-heated to the virial temperature of its dark matter halo host as this latter collapses, and subsequent accreted material encounters the resulting virial shock as it penetrates the halo (Rees & Ostriker 1977; Silk 1977; White & Rees 1978). Since the shock-heated gas is more or less spatially re-distributed as the dark matter before it can cool, one is led to logically postulate that its specific angular momentum closely tracks that of the dark matter halo. Non-radiative hydrodynamics cosmological simulations have confirmed that this is the case (e.g. van den Bosch et al. 2002).

However, as soon as the gas is permitted to radiatively cool and form stars, this tight correlation between gas and dark matter spin should break down. For instance, a fraction of gas accreted at earlier times with lower angular momentum will be converted into stars, elevating the specific angular momentum of the remaining gas (Dutton & van den Bosch 2009). Meanwhile the specific angular momentum of the dark matter halo is expected to either be frozen in after turn around or decline due to the presence of external torques (c.f. Peebles 1969; Book et al. 2011). Hence it is not very surprising that radiative hydrodynamics cosmological simulations show a difference in the spin parameters between gas and dark matter. Indeed, Stewart et al. (2011) have recently reported that for a pair of resimulated halos, cold gas had 3 to 5 times more specific angular momentum than dark matter (see also Sales et al. 2010). In this context, the questions which naturally arise are: (i) what are the mechanisms that segregate dark matter and gas angular momenta? (ii) is this segregation universal or does it depend on halo properties? and (iii) does it evolve with redshift? Since the gas is the main agent for transferring angular momentum from (super) halo scales down to central galaxies, it is key to investigate the evolution of its angular momentum in the region extending between the galaxy and the virial radius of the dark matter halo (i.e. $0.1R_{\rm vir} < r \leq R_{\rm vir}$).

Within galaxy size virialised halos, the picture of gas accretion has recently been significantly revised, with the rediscovery of an idea first put forward by Binney (1977) that infalling gas is never shock-heated to the virial temperature but instead flows through an 'isothermal' shock, reaching the galactic disc cold (Katz et al. 2003; Birnboim & Dekel 2003; Kereš et al. 2005; Ocvirk et al. 2008; Brooks et al. 2009). Moreover, this gas is brought along anisotropic narrow streams which persist deep within the halo, contrary to their broader dark matter counterparts which rapidly fade away at the virial radius (Powell et al. 2011). Therefore, one wonders how differently this filamentary gas advects angular momentum throughout the halo.

With such questions in mind, we use a set of high-resolution cosmological simulations to revisit two key assumptions of disc formation theory, namely that gas carries the same amount of specific angular momentum as its host dark matter halo and that this specific angular momentum is conserved as this material gets accreted onto the central disc. The details of the simulations are described in Section 2. In Section 3, we present the time evolution of angular momentum of baryons and non-baryonic matter along with a comparison to observational data at $z = 0$. We also discuss in this section how our results depend on halo properties and evolve with redshift. Finally, we discuss the discrepancy between dark matter and gas specific angular momenta in Section 4 and conclude in Section 5.

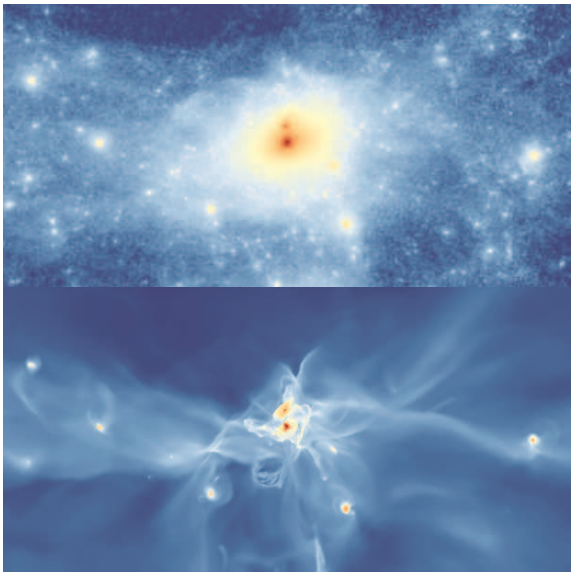

Figure 1. Projected densities of the dark matter (top) and gas (bottom) centred on a halo of $\simeq 10^{11}\,M_{\odot}$ at $z = 3$ from the NUT simulation with supernova feedback (NutFB). A $6R_{\rm vir}$ region is projected and a figure with aspect ratio 1:2 is displayed, where the longer length corresponds to $= 6R_{\rm vir}$ ($= 224$ kpc). At $z = 3$ the scale-height of the disc as well as the large scale filamentary structure is well resolved in the simulation. It can be seen that dark matter filaments are broader than gas filaments. The gas filaments are not destroyed by supernova explosions.

2 SIMULATIONS

We use the Eulerian AMR code, RAMSES (Teyssier 2002), to investigate the angular momentum evolution of baryons and dark matter. RAMSES uses a second-order Godunov scheme to solve the Euler equations, and an adaptive particle-mesh method to solve the Poisson equation. Since the outcome of hydrodynamics simulations is subject to resolution and physical ingredients, we make use of five simulations to draw robust conclusions. These simulations include the NUT series (Powell et al. 2011), the HORIZON-MareNostrum simulation (Ocvirk et al. 2008; Devriendt et al. 2010), and two other cosmological simulations (Cosmo25, Cosmo50, Dubois et al. *in prep.*) of fairly large volumes but with lower resolution than the HORIZON-MareNostrum simulation. Whereas simulations in the NUT series focus on the evolution of an individual, Milky Way-like galaxy, the HORIZON-MareNostrum, Cosmo25 and Cosmo50 simulations give the statistical properties of galaxies spanning a wide range of halo mass. Physical ingredients common to most of our simulations include reionisation, cooling, star formation and supernova feedback. These are summarised in Table 1, along with simulation parameters.

To model the reionisation of the Universe, a uniform UV background radiation field (modelled as a heating term in the energy equation) is turned on at high redshift (see Table 1) following Haardt & Madau (1996). Gas dissipates energy through atomic cooling down to 10^4K (Sutherland & Dopita 1993). For the NUT

simulations metal line cooling can lower the gas temperature further (below ~ 10 K). When the gas density in a grid cell exceeds a given threshold ($n_{\rm th}$, see Table 1), star particles are spawned by a Poisson process according to a Schmidt law with a 1% efficiency of the star formation per free-fall time (Kennicutt 1998; Dubois & Teyssier 2008). This threshold density is chosen so that it is inferior or equal to the maximal Jeans density reached on the finest level. In the simulations with supernova feedback, after ~ 10 Myrs, massive stars undergo Type II supernova explosions, releasing half of their 10^{51} ergs into their surroundings as kinetic energy and the other half as thermal energy (Dubois & Teyssier 2008). During this phase, processed heavy elements are dispersed, enriching the interstellar and intergalactic medium. In what follows, we elaborate on the details of each simulation.

The NUT series make use of the resimulation (also called 'zoom') technique to follow the evolution of a Milky Way-type galaxy in a ΛCDM cosmology. Powell et al. (2011) reported on high redshift results (z $\geq$ 9) from the ultra-high resolution resimulations in the NUT series. These reached a maximum physical spatial resolution of $\sim$ 0.5 pc at all times. To track the evolution of the galaxy down to lower redshifts, the NUT suite also includes three resimulations with lower *spatial* resolution (but identical DM particle mass resolution) and the following physics: (i) adiabatic with a uniform UV background turned on instantaneously at z= 8.5 (NutAD) (ii) cooling, star formation, and UV background (NutCO) and (iii) same as (ii) but with supernova feedback and metal enrichment (NutFB). NutAD and NutCO have maximum 48 pc (physical) resolution at all times and reach $z = 0$, whereas NutFB has maximum 12 pc (physical) resolution and only reaches $z = 3$. Fig. 1 shows a snapshot of the DM (upper panel) and gas (lower panel) of a region centred on a halo hosting a Milky Way-type galaxy at $z = 3$ in NutFB.

We recall the important details of the NUT resimulations here. The simulation volume is a $9h^{-1}$ Mpc comoving periodic box evolving according to a WMAP5 cosmology (Dunkley et al. 2009) ($\sigma_8 = 0.8$, $\Omega_m = 0.258$, $\Omega_\Lambda = 0.742$, $h \equiv H_0/(100{\rm kms}^{-1}{\rm Mpc}^{-1}) = 0.72$). Initial conditions are generated using `MPgrafic` (Prunet et al. 2008), a parallel version of the Grafic package (Bertschinger 2001). Within this volume we identify the region where a Milky Way-like galaxy (halo virial mass of $\simeq 5 \times 10^{11}$M$_\odot$ at $z = 0$) will form. This region encompasses a volume of side length $\sim$ 2.7 h^{-1} Mpc. While the root grid for the entire simulation volume is 128^3, within the ($\sim$2.7 h^{-1} Mpc)^3 region, we place an additional three nested grids, giving an equivalent resolution of 1024^3 dark matter particles, each with mass M$_{\rm DM}$ $\simeq 5 \times 10^4 M_\odot$. To fix the maximum physical resolution to a constant value (12 pc for NutFB and 48 pc for NutCO and NutAD) as the universe expands and the simulation evolves, we further refine on the finest fixed grid within the 2.7 h^{-1} Mpc^3 region according to a quasi-Lagrangian strategy, i.e. when the number of dark matter particles in a cell reaches 8 or equivalently when the baryon plus dark matter density in a cell increases by a factor of 8. Table 1 lists the maximum level triggered for each simulation. Because of the higher spatial resolution in NutFB it uses a higher density threshold for star formation ($n_{\rm H,th} = 400$ cm^{-3}) than the NutCO run ($n_{\rm H,th} = 10$ cm^{-3}). The star particle mass ($\simeq 2 - 3 \times 10^4 M_\odot$) is determined by the combination of minimum grid size and density threshold for star formation (Dubois & Teyssier 2008). In NutFB, we assume that every supernova bubble with an initial radius of 32 pc sweeps up the same amount of gas as that initially locked in the star particles. This is usually expressed as a mass loading factor of unity ($\eta = 1$).

The other three simulations are large volume cosmological simulations, and as such are performed with lower spatial (1–2 kpc) and mass resolution. More specifically, the mass of each dark matter particle is $m_{\rm DM} \simeq 10^7 M_\odot$ for the HORIZON-MareNostrum simulation, $8 \times 10^7 M_\odot$ for the intermediate size run (Cosmo25) and $6 \times 10^8 M_\odot$ for the Cosmo50 run. As in the NutFB run, supernova feedback and UV background heating are included in the simulations, but the radius of the initial supernova bubble is set to twice the minimum size of the grid (see Table 1). Note also that the adopted cosmology for the HORIZON-MareNostrum simulation (WMAP1) is different from the others, but as we will show this has very little impact on our results, if at all. We refer interested readers to Ocvirk et al. (2008) and Devriendt et al. (2010) for a detailed description of the HORIZON-MareNostrum simulation set-up.

In all the simulations, we identify (sub) haloes using the ADAPTAHOP algorithm (Aubert et al. 2004), which is based on the detection of peaks and saddle points in the dark matter density field, supplemented by the most-massive subhalo algorithm developed by Tweed et al. (2009). The virial radius of halos is defined as the maximal radius within which the virial theorem is satisfied to better than 20%. We further define gas belonging to a satellite galaxy as gas residing within the half-mass radius of its host DM satellite halo. The centre of a halo, which we use to compute angular momentum, is defined as the centre of mass of dark matter and baryons. The mean motion of the halos is determined by computing the centre of mass velocity of dark matter particles, gas, and stars within their virial radii.

3 THE ANGULAR MOMENTUM OF VIRIALIZED HALOS

To understand how galaxies acquire their angular momentum, we study the angular momentum evolution of the different components (gas, dark matter, stars) inside their host halos. We compute the specific angular momentum vectors as:

$$\vec{\mathbf{j}} = \frac{\sum_i m_i \vec{\mathbf{r}}_i \times \vec{\mathbf{v}}_i}{\sum_i m_i}, \quad (1)$$

where $\vec{\mathbf{r}}_i$ is the radial distance from the centre of mass of the halo (includes dark matter and baryons), $\vec{\mathbf{v}}_i$ is the peculiar velocity and m_i is the mass of the i-th dark matter (star) particle or gas cell. In what follows we use different subscripts to denote the specific angular momentum of different components in different regions of the halo. These are summarised in Table 2.

3.1 Adiabaticity and the cosmic origin of angular momentum

We begin our investigation of the evolution of angular momentum of the various components of a virialized halo with the simplest (in terms of physics) high resolution NutAD run. Since gas cannot cool radiatively in this simulation, newly accreted material is shock heated by the pressure supported intra-halo medium. As a result, its radially oriented initial velocity is isotropized, and drives the gas density field towards spherical symmetry. Accreted dark matter particles are also more or less isotropically redistributed within the host halo by the collisionless violent relaxation process. Given that (i) gas and dark matter within the halo experience the same larger-scale torques (e.g. Peebles 1969; Book et al. 2011), and (ii) gas and dark matter are driven by the gravitational collapse to a very similar equilibrium distribution (i.e. to a good approximation that of an isothermal sphere since the total amount of angular momentum

Table 1. Summary of simulation parameters and physical ingredients. From left to right, columns are as follows: simulation name, comoving box size, number of dark matter particles, level of the root grid, level of the finest grid, minimum grid size, dark matter particle mass, star particle mass, threshold density for star formation, redshift down to which the simulation is carried out, indication of whether supernova feedback is included, redshift at which UV background heating is initiated, and remarks.

Simulations	L (Mpc/h)	$N_{\rm DM}$	$l_{\rm min}$	$l_{\rm max}$	$\Delta x_{\rm min}$ (pc)	$m_{\rm DM}$ ($M_\odot$)	$m_{\rm star}$ ($M_\odot$)	$n_{\rm th}$ (H/cm^3)	$z_{\rm end}$	SN	UV	Remarks
NutFB	9	1024^3	7	20	12	5×10^4	2×10^4	400	3	Y	z=8.5	Resimulation
NutCO	9	1024^3	7	18	48	5×10^4	3×10^4	10	0	–	z=8.5	Resimulation
NutAD	9	1024^3	7	18	48	5×10^4	–	–	0	–	z=8.5	Resimulation
MareNostrum	50	1024^3	10	16	1090	1×10^7	2×10^6	0.1	1.5	Y	z=8.5	
Cosmo25	25	256^3	8	15	1090	8×10^7	4×10^6	0.1	0	Y	z=10.5	
Cosmo50	50	256^3	8	15	2180	6×10^8	3×10^7	0.1	0	Y	z=10.5	

Table 2. Notations (first column) for specific angular momenta used in this study. The first subscript indicates the component used for the calculation (DM, gas, stars, baryons). The second column specifies the region (normalised to the halo virial radius) over which the specific angular momentum is calculated. The default region over which we measure specific angular momentum is a sphere extending from the centre of mass of the halo to the virial radius. A second subscript indicates whether we exclude ($j_{\rm gas,out}$) or include ($j_{\rm gas,cen}$) the gas in the central region ($r/R_{\rm vir}\leq0.1$) of the halo for the specific angular momentum calculation. The third column lists the components included in the specific angular momentum calculation.

Notation	Spatial extent	Component
$j_{\rm dm}$	$r/R_{\rm vir}\leq1$	dark matter
$j_{\rm gas}$	$r/R_{\rm vir}\leq1$	gas
$j_{\rm gas,out}$	$0.1\leq r/R_{\rm vir}\leq1$	gas
$j_{\rm gas,cen}$	$r/R_{\rm vir}\leq0.1$	gas
$j_{\rm star}$	$r/R_{\rm vir}\leq1$	all stars except those in satellite galaxies
$j_{\rm bar}$	$r/R_{\rm vir}\leq1$	all stars (satellite galaxies included) + gas

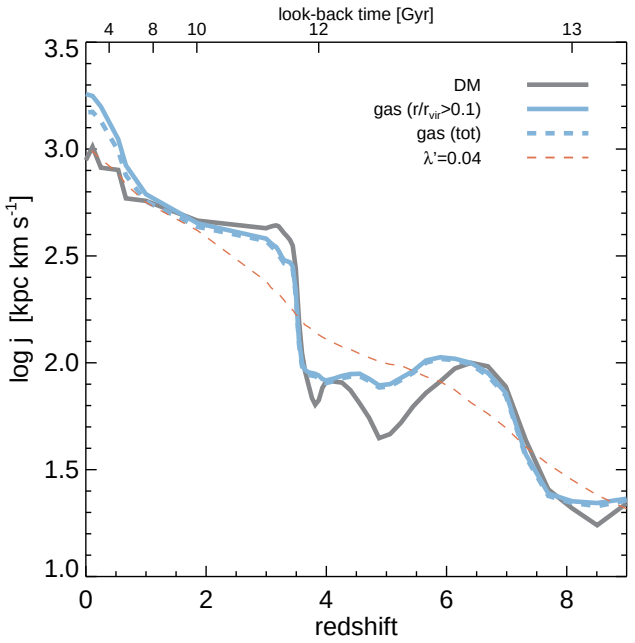

Figure 2. Evolution of the specific angular momentum (j) of a dark matter halo hosting a Milky Way-type galaxy in the adiabatic run (NutAD). Different colours denote different components: dark matter ($j_{\rm dm}$, thick grey), halo gas ($j_{\rm gas,out}$, $0.1\leq r/R_{\rm vir}\leq1$, thick blue). Also plotted as a blue dashed line is j of all the gas inside the virial radius, $j_{\rm gas}$. We also display the specific angular momentum corresponding to a reduced spin value $\lambda'=0.04$ (red dashed line) for the dark matter halo. The specific angular momentum of the halo gas ($j_{\rm gas,out}$) closely follows that of the dark matter halo ($j_{\rm dm}$) in this non-radiative simulation.

provided by tidal torques is very limited), we expect them to have similar j. Indeed, Fig. 2 shows that $j_{\rm gas,out}$ closely tracks $j_{\rm dm}$ regardless of whether or not mergers, easily identified by large jumps in j, occur. When the dark matter angular momentum is expressed in terms of the spin parameter ($\lambda'=j_{\rm dm}/\sqrt{2}R_{\rm vir}V_{\rm c}$, Bullock et al. 2001), we recover the typical value of $\lambda'\simeq0.04$ *at all times* with fluctuations of up to a factor of ~2 around this value.

An interesting feature in Fig. 2 is that $j_{\rm dm}$ increases with time (albeit at a reduced rate below $z=3$), implying that late infall carries a larger amount of angular momentum. This is not a completely unexpected result given that dark matter haloes are known to experience little evolution of spin parameter with time (e.g. Peirani et al. 2004). As their mass and radius grow, so must their angular momentum. However, it is not trivial to understand *why* the late accretion has larger j. A naive answer is that material with larger angular momentum takes more time to reach the potential well, but this does not explain *how* it acquired such a large angular momentum in the first place. We discuss in detail the cosmic evolution of the angular momentum of halos (which necessarily goes beyond tidal torque theory) in a companion paper (Pichon et al. 2011), but for completeness' sake, we briefly outline the main idea in the paragraph below.

The dynamics of the gas and dark matter flowing along what has been dubbed the 'cosmic web' can be understood as the anisotropic time evolution of the initial gaussian random gravitational field. Cosmological structures originate as peaks in the associated initial density field (Bond et al. 1996), which are connected to other peaks through peak patches. The bulk motion of a peak patch is determined by the gradient of the large-scale potential. The latter also drives the motions of filaments which exist at the intersection of at least three void patches and connect peaks. As a consequence of the asymmetry between voids, the gas and dark matter flowing out of these voids acquire a transverse velocity when they intersect at a filament. This transverse velocity is the seed of a halo's angular momentum which is then advected along the filaments all the way into the halo sitting on the peak. Since the transverse velocity along a filament is constant to zeroth order approximation, the material initially located further away from the peak will naturally contribute more angular momentum. Note that the infall of matter along such filaments will *coherently* contribute an increasing amount of angular momentum as time goes on

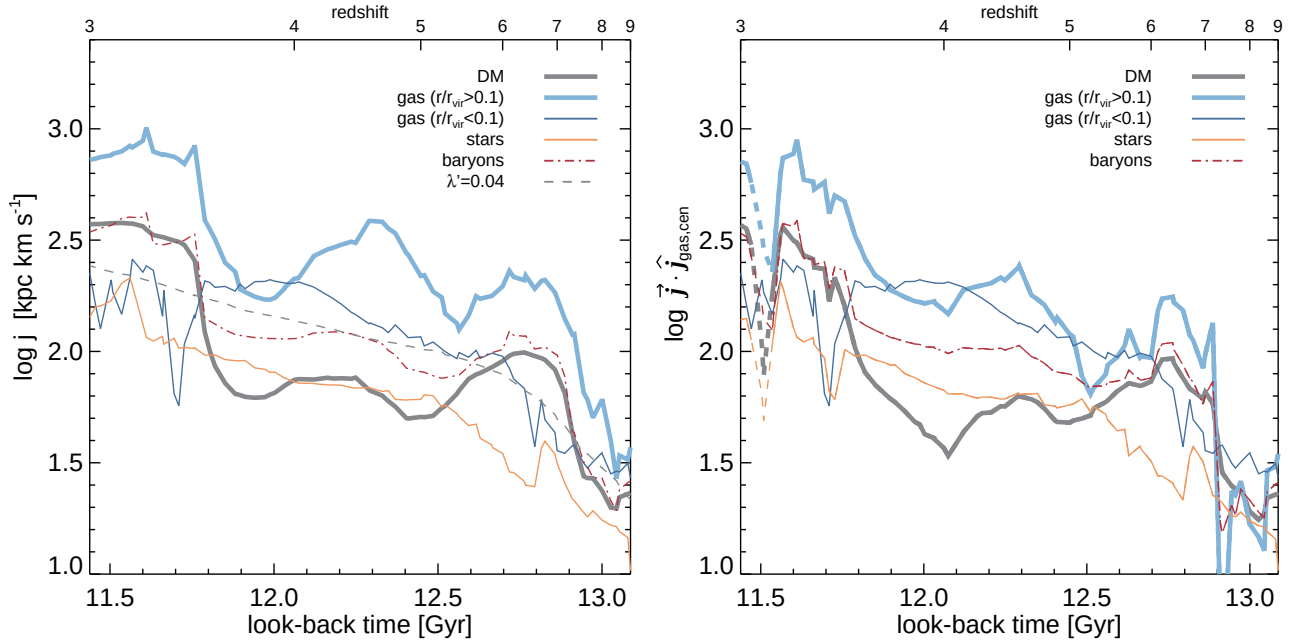

Figure 3. Left panel: evolution of the specific angular momentum modulus (j) from the NutFB run. Different colours denote different components: dark matter ($j_{\rm dm}$, thick grey), gas at $0.1 \leq r/R_{\rm vir} \leq 1$ ($j_{\rm gas,out}$, thick blue), central gas ($r/R_{\rm vir} < 0.1$, $j_{\rm gas,cen}$, thin blue), stars ($j_{\rm star}$, thin orange), all baryons in the halo ($j_{\rm bar}$, dot-dash red). Note that the specific angular momentum calculations for dark matter ($j_{\rm dm}$), gas ($j_{\rm gas,out}$) and baryons ($j_{\rm bar}$) includes the contribution from satellite galaxies, while it is excluded for the measurement of $j_{\rm star}$ and $j_{\rm gas,cen}$. Angular momentum corresponding to a constant reduced spin value of $\lambda' = 0.04$ is included as a grey dashed line. The specific angular momentum of gas ($j_{\rm gas,out}$) is larger than that of its host dark matter halo ($j_{\rm dm}$), suggesting that the angular momentum of the gas is not acquired during the collapse of this latter. Right panel: specific angular momentum along the spin axis of the gas in the central region ($\hat{j}_{\rm gas,cen}$). By definition, $\vec{j} \cdot \hat{j}_{\rm gas,cen}$ for gas in the central region in this panel (thin blue line) is the same as $j_{\rm gas,cen}$ in the left panel. We denote negative values as dashed lines. Different angular momentum amplitudes between lines of the same type in the left and right panels indicate the misalignment between the central gas and each component.

(shown in Fig. 2), since the filament preserves its orientation over long stretches of time.

3.2 Radiative cooling, supernovae feedback, and the evolution of angular momentum at high redshift

In the real Universe, gas can radiatively cool and form stars, which should therefore be considered as a sink for gas mass and angular momentum. Moreover, at high redshift, star formation is very active (Bouwens et al. 2009) and the effect of supernova explosions on the evolution of the halo gas may prove important. Thus, we make use of the high-resolution NutFB run which includes these processes to investigate the evolution of angular momentum of a DM halo at high redshift ($z \geq 3$).

The left panel of Fig. 3 shows that $j_{\rm gas,out}$ and $j_{\rm dm}$ increase steadily, although with occasional rapid variations located around look-back times ($t_{\rm lb}$) of $t_{\rm lb}$ =12.9, 12.4, and 11.7 Gyr. These angular momentum 'jumps' are generated by episodes of enhanced accretion of dense gas contained in satellite galaxies and filaments (e.g. Maller et al. 2002; Peirani et al. 2004). Indeed, the most significant *halo* merger occurs at $t_{\rm lb} \simeq 11.7$ Gyr (satellite to host halo mass ratio $M_{\rm sat}/M_{\rm host} \sim 0.1$) and the majority of the other 12 minor mergers ($0.01 \leq M_{\rm sat}/M_{\rm host} \leq 0.1$) take place between $12.5 \lesssim t_{\rm lb} \lesssim 13.0$ Gyr. In addition to these mergers, material accreted along filaments also contributes to the rapid variation of j since the density in the gas filaments varies (see also Fig. 2 of Brooks et al. 2009).

However, the key feature of Fig. 3 (left panel) is that $j_{\rm gas,out}$, although tightly correlated with $j_{\rm dm}$, is always larger by a factor of a few (see also Chen et al. 2003; Sharma & Steinmetz 2005; Gottlöber & Yepes 2007; Sales et al. 2010; Stewart et al. 2011). This is in contradiction with the picture in which the angular momentum of the halo gas is acquired during the virialisation of its host dark matter halo and suggests that if the gas and the DM halo interact at all and exchange angular momentum during the collapse, the effect is likely to be unimportant, at least in the outer regions of the halo. Indeed this is more in line with the picture according to which gas accreted at the virial radius supersonically streams (almost) directly into the central galaxy (e.g. Brooks et al. 2009; Powell et al. 2011). Moreover, Fig. 3 (left panel) also shows that $j_{\rm gas,cen}$ (thin blue solid line) is systematically smaller than $j_{\rm gas,out}$ (thick blue solid line). There are two possible explanations for this. First, the specific angular momentum *modulus* of the gas is not conserved during its gravitational collapse and subsequent accretion onto the central galaxy because $\vec{\mathbf{j}}_{\rm gas,out}$ is misaligned with $\vec{\mathbf{j}}_{\rm gas,cen}$ (also see van den Bosch et al. 2002; Hahn et al. 2010; Bett et al. 2010). The second possibility is that unlike the gas in the outer part of the halo which yields an instantaneous picture of the accreted angular momentum, the central gas reflects the angular momentum accretion *history* of the gas. We now discuss each of these possibilities in turn.

The difference in angular momentum alignment between outer and inner gas is indicated in the right panel of Fig. 3 where we plot the component of $\vec{\mathbf{j}}_{\rm gas,out}$ (thick solid blue line) parallel to $\vec{\mathbf{j}}_{\rm gas,cen}$. This figure clearly shows that this component is remarkably well preserved (as one would expect for an isolated axisymmetric system) and it is therefore tempting to conclude that misalignment accounts for most of the difference between $j_{\rm gas,out}$

and $j_{\rm gas,cen}$. However, the time evolution of the projected component of $\vec{\mathbf{j}}_{\rm gas,out}$ along $\vec{\mathbf{j}}_{\rm gas,cen}$ direction does not correlate very well with the time evolution of $j_{\rm gas,cen}$. This behaviour is naturally interpreted as a gas accretion history effect. Indeed, as the mass of gas in the low amplitude specific angular momentum central region ($r/R_{\rm vir} \leq 0.1$) is comparable (between a factor 2-3 smaller) to that in the outer reservoir ($0.1 \leq r/R_{\rm vir} \leq 1$) (see Appendix for details on the evolution of the gas mass in these regions), even if $\vec{\mathbf{j}}_{\rm gas,out}$ was perfectly aligned with $\vec{\mathbf{j}}_{\rm gas,cen}$, the resulting modulus of the specific angular momentum of the inner region after accretion would naturally be reduced compared to that of the freshly accreted gas. As a result, notwithstanding mergers, $j_{\rm gas,cen}$ grows more smoothly than $j_{\rm gas,out}$ and takes more time to reach a given level of specific angular momentum. This integrated effect is exacerbated for the stellar component, which displays an even smaller amount of specific angular momentum than $j_{\rm gas,cen}$. Since the global star formation timescale is much longer than the dynamical timescale of the central region (e.g., Kennicutt 1998), most of the stars will form from older gas, with a lower angular momentum amplitude. Even though newly formed stars carry more angular momentum, they represent a smaller fraction of the total stellar mass than the central gas mass compared to that of the total halo gas. Therefore, a supplementary time delay to reach a given level of j and a smoother growth in specific angular momentum amplitude of the stellar component is inevitable (Dutton & van den Bosch 2009).

Finally, when we measure the specific angular momentum of the *total* baryonic component, i.e. gas and stars, ($j_{\rm bar}$: thin red dot-dashed line in the left panel of Fig. 3), we find that its amplitude most closely tracks that of the specific angular momentum of the DM ($j_{\rm dm}$, thick grey solid line) which we know reflects the mass assembly history of the halo. We are not implying that $|\vec{\mathbf{j}}_{\rm dm}|$ of individual dark matter particles is conserved during the collapse, but simply that, as the baryon angular momentum is advected deep within the halo, we can only probe the accretion history of the gas by including all baryons within the inner region. When this effect is accounted for, there is no indication in our simulation that baryons lose more (or less) specific angular momentum amplitude than DM during gravitational collapse of the halo. Interestingly, the specific angular momentum of the central gas has a value close to that of dark matter for virialised halos typically measured in N-body simulations ($\lambda' = 0.04$) (e.g. Efstathiou & Jones 1979; Barnes & Efstathiou 1987). It should be noted, however, that it is established with the aid of gas within $0.1 \leq r/R_{\rm vir} \leq 1$, which has a larger j than the dark matter. We therefore surmise that if this gas had started with the same specific angular momentum as the dark matter halo to begin with, the central gas would have been left with roughly half of the typical DM specific angular momentum. We come back to the crucial issue of specific angular momentum segregation between gas and DM in Section 4 but now address the question of the importance of feedback in regulating $j_{\rm gas,cen}$.

Using a couple of cosmological hydrodynamics resimulations, one of a bulge-dominated galaxy and another of a disk-dominated galaxy at redshift 0, Zavala et al. (2008) show that the specific angular momentum of the disc galaxy closely follows that of its dark matter halo. They argue that this is because the stellar feedback in the simulation which produces the disk-dominated galaxy is strong enough to heat the gas within the halo thereby preventing it from cooling too much at early times, fragmenting into subgalactic clumps, and transferring its angular momentum to the dark matter halo by dynamical friction. Instead this hot gas accumulates in the halo where it acquires the specific angular momentum of

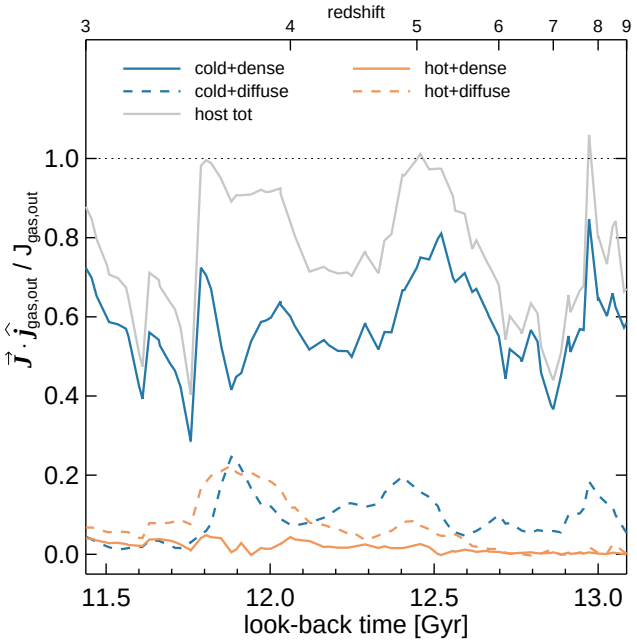

Figure 4. Fraction of total angular momentum of gas at $0.1 \leq r/R_{\rm vir} \leq 1$ from various components. We divide the gas into four different phases: i) cold ($T < 10^5$K), dense filamentary ($n_{\rm H,fil} \leq n_{\rm H} < n_{\rm H,th}$), ii) cold diffuse ($n_{\rm H} < n_{\rm H,fil}$), iii) hot ($T > 10^5$K) dense, and iv) hot diffuse component (see Equation (2) for the definition of $n_{\rm H,fil}$). Note that these quantities do not include the gas belonging to satellite galaxies. Grey solid line corresponds to the total fraction of angular momentum of gas belonging to the host halo. Cold, dense filamentary accretion accounts for most of the angular momentum in the halo.

the dark matter before it eventually cools and re-collapses onto the central galactic disc, all the while conserving its angular momentum. However, in the first cosmological resimulation where individual supernovae remnants are resolved, very little gas is heated by stellar feedback at high redshift (Powell et al. 2011). Moreover, these authors show that the cold filaments which supply most of the gas to the galaxy (Kereš et al. 2005, 2009; Dekel & Birnboim 2006; Ocvirk et al. 2008; Brooks et al. 2009) are not disrupted by supernova feedback. This result has been independently confirmed by Faucher-Giguere et al. (2011) who used the constant velocity wind model of Springel & Hernquist (2003) to model feedback and found that at high redshift ($z \geq 3$) their supernova-driven galactic winds with low mass loading ($\eta = 1$) were not able to suppress the accretion of cold, dense gas in intermediate-mass haloes ($M_{\rm vir} \sim 10^{11-12}\ M_\odot$). Only when they assumed extreme parameters for their wind (i.e. loaded them with double the mass that is turned into stars, and drove them with double the amount of energy than that available from their supernova explosions) were they able to shut down cold, dense accretion. However this took place at the expense of the baryonic mass function which ended up dramatically undershooting the observations of e.g. Bell et al. (2003) at $z = 0$. Purely based on energetic grounds, feedback from active galactic nuclei may be able to blast the filamentary structure (van de Voort et al. 2010), but it is unclear how geometrical effects will affect their capacity to do so. A collimated jet for instance will not, in general, deposit enough of this energy in the vicinity of the filaments because of their small covering factor (a few percent, Kimm et al. 2011). In any case, in the simulation presented here, and contrary to the conclusions of Zavala et al. (2008), the specific

angular momentum of the gas *in the galaxy* (thin blue line in the left panel of Fig. 3) is similar (slightly larger) to that in its DM halo host, even though supernova feedback is moderate. This raises the question of the importance of the numerical technique employed to assess the fragmentation and transfer of angular momentum in disks. Although this is beyond the scope of this paper, as we are chiefly interested in the outer parts of the halo, we believe that our simulation provides a more correct answer simply because we have better resolution. We refer the interested reader to the recent paper by Commerçon et al. (2008) for a thorough comparative study between SPH and AMR as to how a high artificial viscosity and numerical noise undermine the capacity of the SPH technique to conserve angular momentum of disks when the number of particles (total and in the kernel) is not high enough.

Since accretion through cold, dense filamentary gas is thought to dominate at high redshift (e.g. Brooks et al. 2009; Powell et al. 2011), the larger $j_{\rm gas,out}$ relative to $j_{\rm dm}$ is also expected to be associated with the dense filamentary component. To test this idea, as well as assess the importance of supernova feedback, we divide the gas into four different phases according to temperature and density as

(i) cold dense ($T < 10^5$K and $n_{\rm H,fil} \leq n_{\rm H} < n_{\rm th}$)
(ii) cold diffuse ($T < 10^5$K and $n_{\rm H} < n_{\rm H,fil}$)
(iii) hot dense ($T \geq 10^5$K and $n_{\rm H,fil} \leq n_{\rm H} < n_{\rm th}$)
(iv) hot diffuse ($T \geq 10^5$K and $n_{\rm H} < n_{\rm H,fil}$).

where we define the cold dense filamentary structure using the $n_{\rm H,fil} \leq n_{\rm H} < n_{\rm H,th}$ gas density cut. The lower density bound ($n_{\rm H,fil}$) is chosen as

$$n_{\rm H,fil} \equiv \delta_{\rm f} \bar{\rho} f_{\rm bar} X_{\rm H} / m_{\rm H}, \quad (2)$$

where $f_{\rm bar}$, $X_{\rm H}$, and $m_{\rm H}$ are the universal baryon fraction ($\Omega_{\rm b}/\Omega_{\rm m}$), the primordial hydrogen mass fraction and the mass of the hydrogen atom, respectively. The dependence of the lower bound of the filament density on the background density ($\bar{\rho}(z)$) is motivated by the fact that the filamentary structure acquires its properties on large scales which are not gravitationally decoupled from the expansion of the Universe. The parameter $\delta_{\rm f}$ determines the overdensity of the filamentary gas. We find that $\delta_{\rm f} \sim 100$ reasonably identifies the filamentary structure in the NUT simulations, which corresponds to hydrogen number densities higher than $n_{\rm H} \simeq 0.02$ and $\simeq 0.001$ cm^{-3} at z=9 and z=3, respectively. Note that, although this is not a worry in the NUT simulations because we spatially resolve the filaments, $\delta_{\rm f}$ will generally be resolution-dependent in cosmological simulations. In a rather obvious fashion, a lack of spatial resolution will artificially broaden the filamentary structure and thus reduce its density as mass needs to be conserved.

Fig. 4 shows the contributions from the four different phases to the *total* angular momentum of the gas located at $0.1 \leq r/R_{\rm vir} \leq 1$. We emphasize that gas belonging to satellite galaxies is excluded from the measurements. It is clear from this figure that cold filamentary accretion is primarily responsible for the larger $j_{\rm gas,out}$. The cold filamentary gas alone accounts for more than half of the gas angular momentum in the region. Thus, it can safely be concluded that the cold, dense filamentary accretion carries material with larger j than the dark matter halo from outside the virial radius to the inner region of haloes without the gas having much time at all to interact with the dark matter. Gas belonging to satellite galaxies occasionally contributes a significant fraction of J (difference between the solid grey line and a horizontal line drawn for $\vec{\mathbf{J}} \cdot \hat{j}_{\rm gas,out}/{\rm J}_{\rm gas,out} = 1$ in Fig 4). However, its impact on the specific angular momentum is less significant than that of the cold, dense filamentary accretion at $z \geq 3$ for two reasons. First, whilst cold, dense filamentary gas flows into the central gaseous disc rapidly, gas gravitationally bound to a satellite galaxy orbits around it for the time it takes dynamical friction to drag the satellite galaxy down. As a consequence of this process, satellite gas angular momentum in Fig. 4 cannot be directly converted into the actual angular momentum of gas accreted onto the central galaxy. Second, satellites are accreted along the gas filaments, and hence part of the gas which we conservatively assigned to these satellite galaxies could be regarded as filamentary gas. In this sense, the estimate of J for the satellites in Fig. 4 should be considered as an upper bound, and thus the actual fraction of the total angular momentum contributed by cold filamentary accretion may be slightly higher than reported in this work. Finally, the contribution to the total angular momentum from other phases (hot diffuse, hot dense, and cold diffuse) to J turns out to be minor for a DM halo of this mass in this redshift range. Whilst the lack of angular momentum of the cold diffuse phase originates from its almost isotropic accretion which cancels its angular momentum to a high degree, that of the hot gas phase is mainly caused by the small mass fraction of hot gas. This result is not very surprising because our DM halo, at $10^{11} M_\odot$ is not massive enough to sustain a stable virial shock (Birnboim & Dekel 2003; Kereš et al. 2005), and supernova explosions in simulations are notoriously inefficient at ejecting large amounts of hot gas in the halo (Mac Low & Ferrara 1999; Dubois & Teyssier 2008; Powell et al. 2011; Faucher-Giguere et al. 2011).

3.3 Shock heating and the evolution of angular momentum at low redshift

Gas infall at low redshift is dominated by smooth accretion rather than mergers (e.g. Fakhouri et al. 2010, and references therein). As discussed by Pichon et al. (2011), this substantially increases the specific angular momentum of gas in the halo by delivering it coherently via the large-scale cosmic web. This is illustrated in Fig. 5, where the time evolution of $j_{\rm gas,out}$ for the Milky Way-like halo in the NutCO[1] simulation is found to be smoother at low redshift ($z < 3$) than at high redshift ($z > 3$). The final mass of the dark matter halo in the NutCO run is $M_{\rm vir} \simeq 4 \times 10^{11} M_\odot$ (see Appendix for a time evolution of the halo mass), which is thought to be close to the mass at which gas accretion transitions from the cold mode to the hot mode (Birnboim & Dekel 2003; Ocvirk et al. 2008). Since the NutCO run does not include supernova feedback, satellite galaxies can retain more gas than in the NutFB run, and thus the resulting relative contribution from the cold, dense filamentary gas to the total angular momentum gets slightly smaller at high redshift than the feedback run (Fig. 6). However, there is little difference in $j_{\rm gas,out}$ or $j_{\rm dm}$ between these two runs for $z \geq 3$. Fig. 6 also shows that at $z \lesssim 2$, the diffuse hot gas phase becomes the dominant reservoir of angular momentum in the region ($0.1 \leq r/R_{\rm vir} \leq 1$). Considering that the post-shock temperature for an isothermal sphere of mass a few times $10^{11} M_\odot$ (our halo reaches $2 \times 10^{11} M_\odot$ at $z \simeq 2$, c.f. Appendix A) is $T_{\rm shocked} \gtrsim 3T_{\rm vir}/8 \sim 10^5$K (Dekel & Birnboim 2006), where $T_{\rm vir} (\simeq 35.9 \times (V_c/[{\rm km \cdot s^{-1}}])^2)$ is the virial temperature, and that the run does not feature any SN feedback, we can safely identify the halo hot gas at $z \lesssim 2$ with material which has been shock-heated.

[1] Run with identical initial conditions and mass resolution to the NutFB run discussed in the previous subsection, but with lower (48 pc) spatial resolution and no supernova feedback

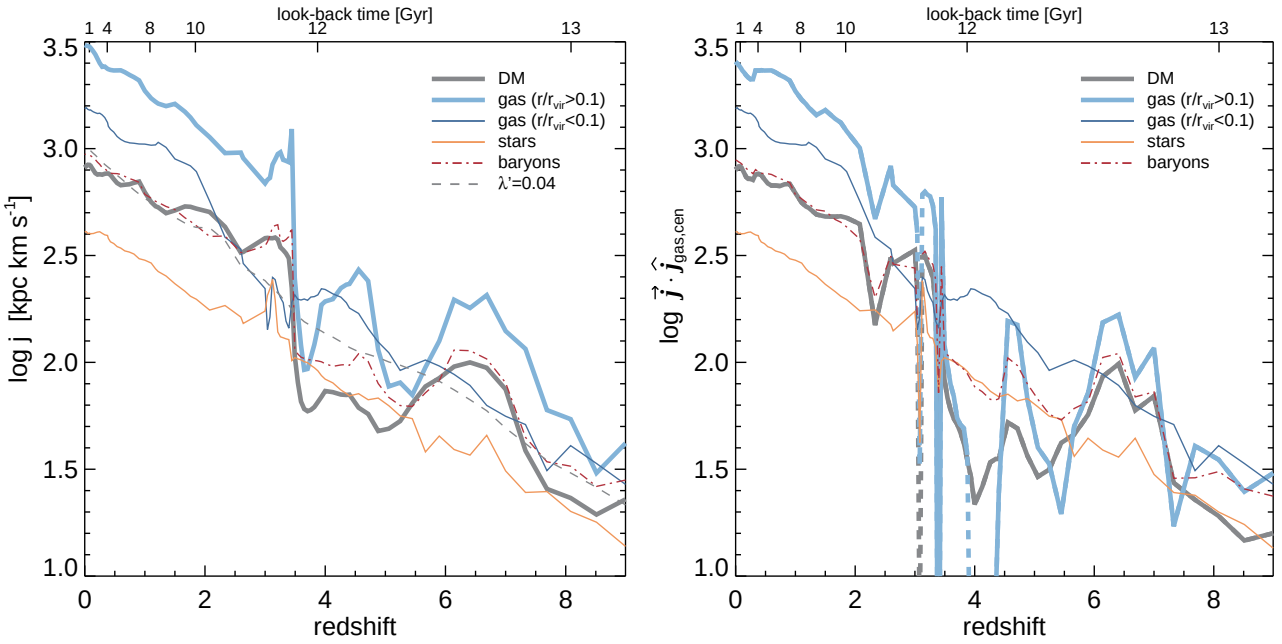

Figure 5. Same as Fig. 3, but for the NutCO run. Different colours denote different components: dark matter (thick grey), gas at $0.1 \leq r/R_{\rm vir} \leq 1$ (thick blue), central gas ($r/R_{\rm vir} \leq 0.1$, thin blue), and stars (orange). Note that the dark matter halo and the halo gas includes the contribution from satellites, while they are excluded for the measurement of j of stars. We also display j of all baryons (star+gas) as a red dot-dashed line. Specific angular momentum corresponding to $\lambda' = 0.04$ is included as a grey dashed line. At low redshift, the misalignment between the central gas and each component is small, and gas in the outer region shows larger angular momentum than dark matter in both panels.

Nonetheless, as Fig. 5 clearly demonstrates, this hot halo gas within $0.1 \leq r/R_{\rm vir} \leq 1$ still has a specific angular momentum higher than that of the dark matter, indicating that shock-heating of the accreted cold gas, even when it takes place as early as $z = 2$, does not erase the difference in specific angular momentum of dark matter and gas.

As is the case in the NutFB run, we find that $j_{\rm bar}$ is comparable to $j_{\rm dm}$ up to z=0, whilst $j_{\rm gas,out}$ is always greater than $j_{\rm dm}$. Once again, given that gas accretion at the virial radius of the halo is never perfectly coplanar with the galactic disc, we expect the (small) off-axis components (j_x and j_y) to vanish before gas becomes part of the central galaxy, and thus the modulus of gas specific angular momentum not to be conserved in general. We also expect gas accretion history to reduce the modulus and smooth the time evolution of $j_{\rm gas,cen}$with respect to $j_{\rm gas,out}$. Fig. 7 shows the radial profiles of the j distributions of gas and dark matter within the virial radius of the dark matter halo, normalised to their respective values of j at $0.1R_{\rm vir}$. These profiles are split in a low and a high redshift bin ($z \leq 3$ and $z > 3$) and stacked. Two striking features emerge from the analysis of Fig. 7. First the dependence of the shape of *all* the specific angular momentum profiles on redshift is minor. Second, while the j of the dark matter component drops almost proportionally with radius, the j profile of the gas is flat in the outer parts of the halo ($r \geq 0.1\ R_{\rm vir}$). Although we did not included the curve in this paper, this is in stark contrast with the behaviour of the gas specific momentum in the NutAD run which closely follow the j profile of the dark matter halo. This implies that as long as the gas can radiatively cool, its specific angular momentum is conserved whilst it is being advected to the inner region ($r < 0.1\ R_{\rm vir}$), regardless of whether shock heating occurs or not. Therefore, any redistribution of angular momentum must happen within the central region of the halo, close to the galactic disc. The detailed analysis of this complex process is beyond the scope of the current paper and will be presented elsewhere (Tillson et al. *in prep.*).

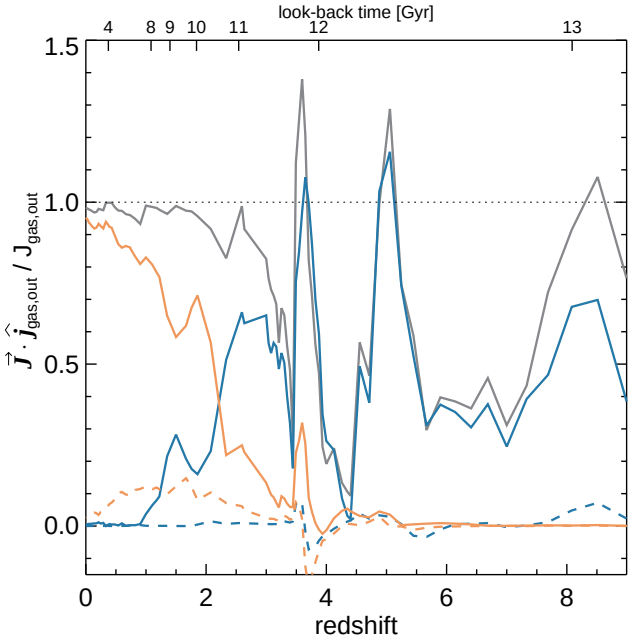

Figure 6. Same as Fig. 4, but for the NutCO run. The hot gas phase (orange lines) begins to develop at $z \sim 3$, and accounts for almost all of the angular momentum in $0.1 \leq r/R_{\rm vir} \leq 1$ by $z = 0$.

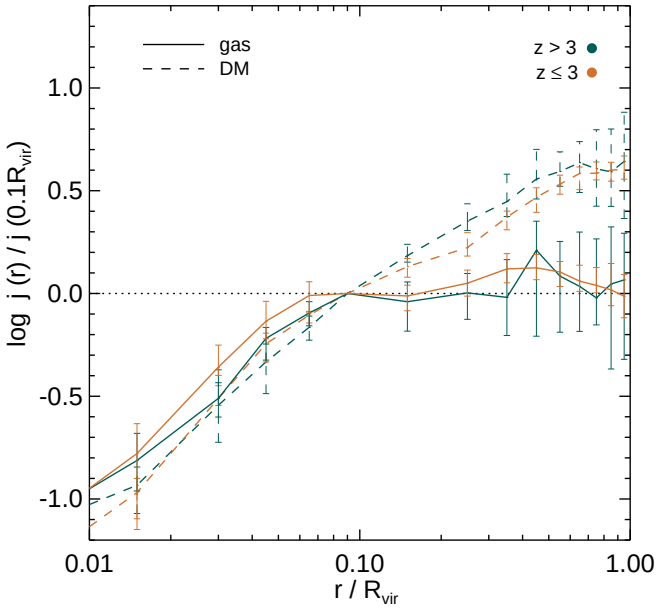

Figure 7. Stacked distributions of normalised specific angular momentum as a function of radius from the NutCO run. The specific angular momentum of gas and dark matter is shown as solid and dashed lines. Blue lines display j at high redshift ($z > 3$), while orange lines show j at low redshift ($z \leq 3$). Each point corresponds to the median, and interquartile ranges are included as error bars. The normalised j of gas is flat at $0.1 \lesssim r/R_{\rm vir} \lesssim 1$, and gets diminished in the region where the galactic disc is located, suggesting that j of gas is reasonably conserved up to $r = 0.1R_{\rm vir}$.

3.4 Generalisation of the results

Now that we have established that gas in a Milky Way-like halo has a larger specific angular momentum than dark matter, it is vital to know whether this property is generic or not. To build a statistically representative sample of haloes, we make use of three large cosmological hydrodynamics simulations called HORIZON-MareNostrum, Cosmo25, and Cosmo50. The HORIZON-MareNostrum simulation contains 326, 1921, 3307, and 4015 haloes with $M_{\rm vir} \geq 10^{11} M_{\odot}$ at z=6.1, 3.8, 2.5, and 1.5. Since the simulation has only been carried out down to z=1.5, we use the Cosmo25 and Cosmo50 run to supplement the sample at lower redshifts. The number of haloes with $M_{\rm vir} \geq 10^{11} M_{\odot}$ in the Cosm25 run is 378 and 459 at z=1.5 and z=0 respectively. For the Cosmo50 run, we restrict our analysis to 481 more massive haloes ($M_{\rm vir} \geq 10^{12} M_{\odot}$) at z=0 because of the poorer resolution of the simulation.

The middle panel of Fig. 8 shows the median and the interquartile range of the spin parameter distribution of the dark matter haloes. As is well known in the literature, it shows that the typical value for the spin is $\lambda \simeq 0.04$ with very little dependence on halo mass and redshift. On the other hand, the spin parameter of gas in the HORIZON-MareNostrum simulation (filled circles) is 2–4 times higher in general than that of the dark matter halo and clearly depends on halo mass. The ratio turns out to be even more significant at z=0 in the Cosmo25 (asterisks) and Cosmo50 run (diamond), demonstrating that our finding that gas has larger specific angular momentum extends to *all* halos over the *entire* redshift range. Moreover, it also substantiates our claim that gas brought in later in the life of the halo has more specific angular momentum because of the large scale origin of this angular momentum which has been investigated in a companion paper (Pichon et al. 2011). Note

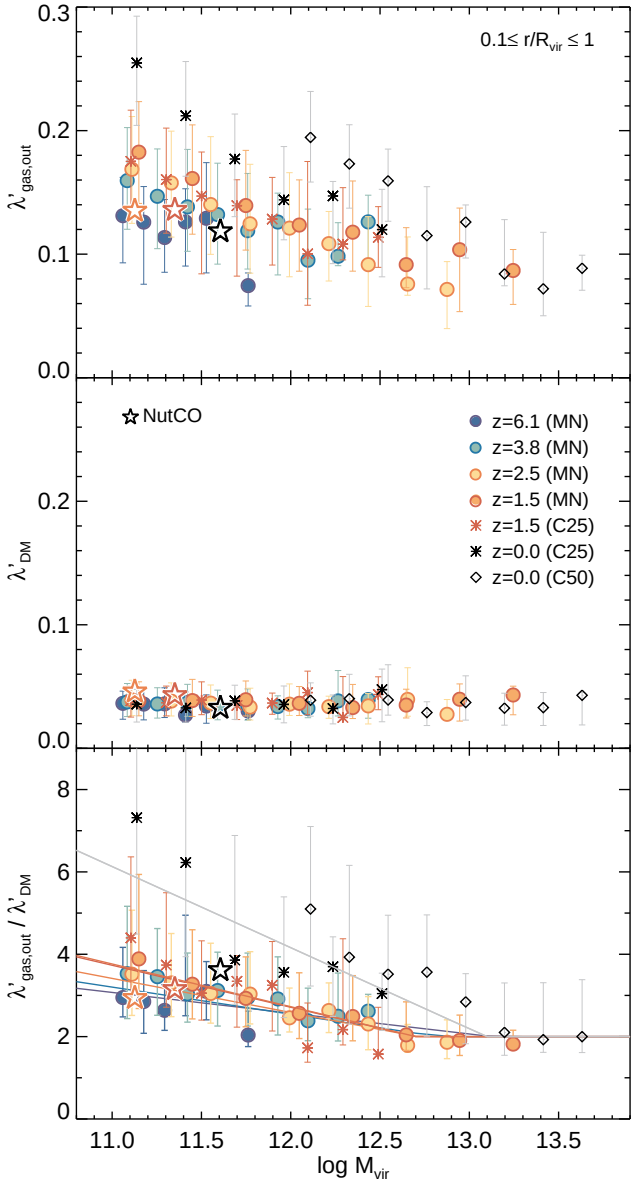

Figure 8. Spin parameter distributions of the gas within $0.1 \leq r/R_{\rm vir} \leq 1$ (top), the dark matter halo (middle), and the ratio of the two (bottom). Filled circles correspond to the results from the HORIZON-MareNostrum simulation, and asterisks and diamonds show the results from the Cosmo25 and Cosmo50 run, respectively. Different colours denote different redshifts as indicated on the figure. The results from the NutCO run are also included as stars with the same colour-coding. Solid lines show linear fits to the simulated data at different redshifts as given by Equation (3). Statistically, the specific angular momentum of the gas within $0.1 \leq r/R_{\rm vir} \leq 1$ is at least twice that of the dark matter halo host, at all redshifts.

that since the HORIZON-MareNostrum and Cosmo25 simulations are run using different cosmologies (WMAP1 and WMAP5 respectively) and feature different mass resolutions, we included data at a common redshift ($z = 1.5$) to ensure that the differences between the z=1.5 HORIZON-MareNostrum and the z=0 Cosmo25 halos does not arise from a different choice of cosmology/simulation parameters.

For practical purposes, we compute a redshift-dependent fit to the specific angular momentum gas to dark matter ratio for halos with $M_{\rm vir} \leq 10^{13} M_{\odot}$

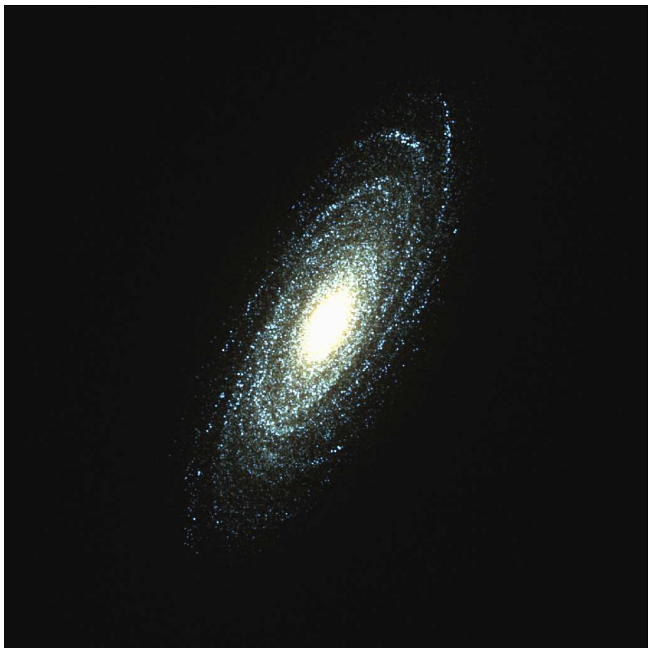

Figure 9. True colour composite image of the NutCO galaxy in the U, B and V at $z = 0$. The image measures 15 kpc on a side. Note that internal extinction by dust is not accounted for in this image. Notice the presence of a large bulge (I-band B/D ratio 0.78) typical of a galaxy with morphological type Sa/b (see text for detail).

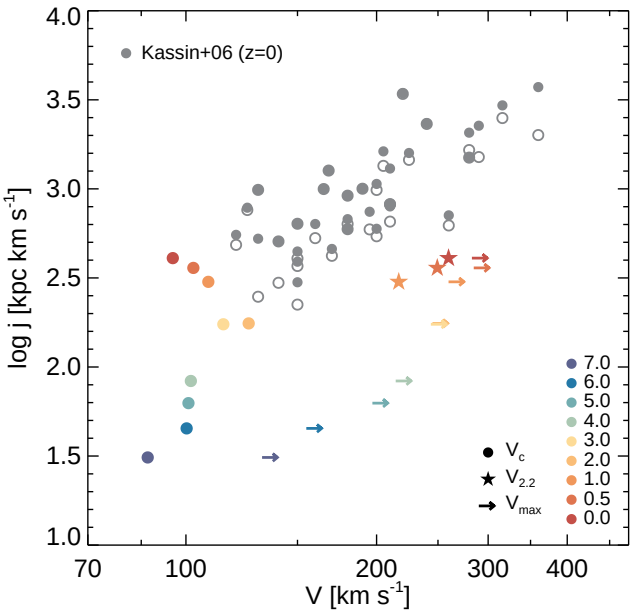

Figure 10. Comparison between the NutCO galaxy and the observational bright disc galaxy sample described in Kassin et al. (2006). Observational data is in grey (lower and upper estimates of j are given by empty and solid circles respectively, see Kassin et al. 2011 for details). For the simulation data, different symbols (circles and right arrows) stand for different estimates of the velocity of the galaxy (circular velocity and maximum rotation velocity). We also include estimates of $V_{2.2}$, the velocity measured at 2.2 times the exponential scale length in I band, for $z \leq 1$. Note that the simulated galaxy displays a dense large bulge which overgrows, at least partially, because of the lack of modelling of any kind of internal feedback (radiation, stellar winds, supernovae, cosmic rays, etc.) in the NutCO run.

$$\frac{\lambda'_{\rm gas,out}}{\lambda'_{\rm DM}} \simeq \max[3.5{+}24.3(1{+}z)^{-0.8} - 1.97(1{+}z)^{-0.7} \log M_{\rm vir}, 2]. \quad (3)$$

We emphasize that all the extra specific angular momentum brought in by the gas will not be devoted to spinning up the central galactic disc, given that its typical misalignment with the central gaseous disc is measured to be $\approx 40^\circ$ for intermediate mass halos ($M_{\rm vir} \sim 10^{11} M_\odot$) in the HORIZON-MareNostrum simulation. Moreover, in the vicinity of the central disc, hydrodynamical interactions with the circum-galactic gas will become important and may substantially redistribute angular momentum. A careful numerical investigation of angular momentum advection in the central region is therefore needed to determine whether or not a simple semi-analytic approach is capable of correctly describing the evolution of angular momentum of disc galaxies using the new initial conditions we provide with this fit.

We also note that limited spatial resolution of our large volume cosmological simulations will lead to an artificial increase of the gas angular momentum, especially in low mass halos. Indeed, the softening of the gravitational force produces very extended discs at the centre of these halos, which would probably be contained within 0.1 $R_{\rm vir}$ at higher resolution. However, comparing the spin of the gas in the NutCO halo (large empty stars in Fig. 8) at various redshifts with that measured for a sample of halos of comparable mass available in these cosmological simulations (solid circles and asterisks in Fig. 8), we conclude that resolution effects most likely account for a minor fraction of the gas spin ($\sim 20\%$).

3.5 Comparison with observations

Ultimately, to decide whether or not our simulations yield realistic galaxies, we have to compare their properties with observations. Unfortunately, with the high resolution we need to properly address the issues related to angular momentum, cooling and feedback, we can only perform such a comparison at $z = 0$ with one of our runs (NutCO) at the time being. As this simulation does not model any feedback mechanism, by z=0 the simulated galaxy has formed too many stars ($M_{\rm star} = 6.8 \times 10^{10} M_\odot$). At $z = 0$, the I-band bulge-to-disc ratio (B/D) of the central galaxy in the NutCO run is $\simeq 0.78$ (see Fig. 9). Such a value is close to the typical B/D of Sa/Sb type spirals, but the disc scale length (2.0 kpc) turns out to be smaller than those observed (Graham & Worley 2008).

Nevertheless, bearing this caveat in mind, we present in Fig. 10 measurements of the j versus V relation for the NutCO galaxy at various redshifts, compared to the observational bright disc galaxy sample gathered by Kassin et al. (2006) (at $z \simeq 0$). Kassin et al. derived the specific angular momenta for these galaxies from Halpha + HI rotation curves and radial stellar mass distributions given in (Kassin et al. 2006). The average errors in j measured from the data are $\approx 60\,{\rm kpc\,kms}^{-1}$. As is done in the observations, both the amount of specific angular momentum and the velocity of the simulated galaxy ($V_{\rm max}$, maximum of the rotation curve) are estimated using the stellar component, except for the filled circle symbols where the velocity is measured as the circular velocity at the virial radius of the dark matter halo. For a fair comparison with observations, we also include velocities measured at 2.2 times the disc scale length in the I band ($V_{2.2}$) at $z \leq 1$.

Looking at Fig. 10, one clearly sees that the velocity estimate plays a crucial role in our ability to assess whether simulated galaxy stars have the correct amount of angular momentum. This is be-

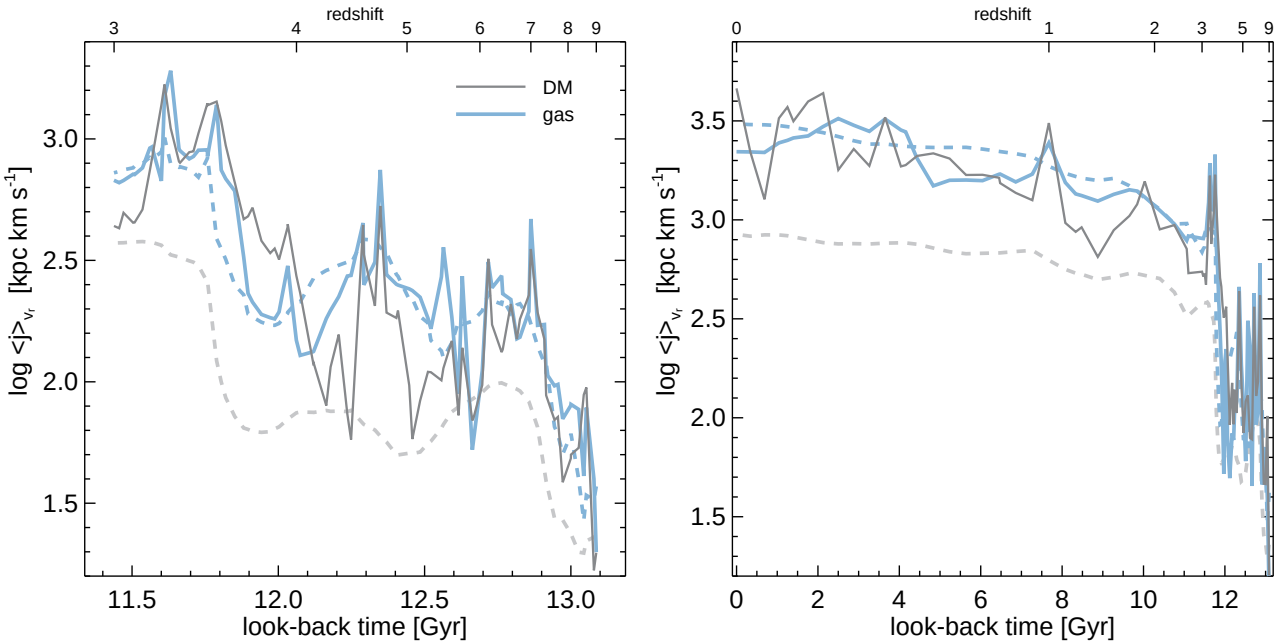

Figure 11. Accretion-weighted specific angular momentum for dark matter (black solid line) and gas (blue solid line) at the virial radius in the NutFB (left panel) and the NutCO (right panel) runs. The specific angular momenta of the dark matter and the halo gas ($j_{\rm gas,out}$) shown in Fig. 3 and 5 are included as grey dashed and blue dashed lines. Note the similar evolution of the specific angular momentum of the halo gas and of both accreted gas and dark matter.

cause the observed slope of the relation (≈ 2) is quite large so any error on the velocity will translate into a much larger error on the specific angular momentum. More specifically, our simulation suffers from forming too many stars and as a result any velocity estimated in the central region of the halo is bound to be too large. If, on the other hand, we use the circular velocity at the virial radius of the halo to bypass the problem (note that this is current practice, see e.g. Dutton & van den Bosch 2009), we find that the level of angular momentum of the simulated stars is in fair agreement with the observations (Fig. 10). We point out that this is a consequence of the lossless transport of a large amount of specific angular momentum by gas from super halo scales right into the inner regions, followed by its redistribution in the vicinity of the disc, as discussed in the previous section. As a result of this effect and the low efficiency of the star formation process on disc scales, stars end up with a factor 2 to 3 less angular momentum than their dark matter halo counterpart which is very close to the discrepancy between dark matter only simulations and observations, as pointed out by Navarro & Steinmetz (2000) and Kassin et al. (2011, *in prep.*).

Finally, it is interesting to note that when we use the $V_{\rm max}$ estimates for the velocity of the galaxy, although we do not match the zero point of the relation, simulated data points at different redshifts move along the observed sequence, suggesting that we would predict very little time evolution of the sequence. On the contrary, $V_{\rm c}$ estimates suggest there exists a strong evolution of the relation with redshift as the flat velocity profile of the dark matter halo is already in place very early on.

4 ORIGIN OF THE DISCREPANCY BETWEEN DARK MATTER AND GAS SPECIFIC ANGULAR MOMENTA

Having robustly demonstrated that the amount of specific angular momentum carried by gas and dark matter differ throughout the virialised halo and at all redshifts, we now turn to identifying the cause of such a difference in j. There are essentially three possibilities: i) the gas carries a larger amount of specific angular momentum than the dark matter at the time of accretion, or ii) the dark matter component does not conserve j as well as the gas or iii) the difference in j reflects a different spatial re-distribution of the angular momentum of gas and dark matter within the virialised halo.

In order to test the first possibility, i.e. whether the gas already carries a larger amount of specific angular momentum than the dark matter when it is accreted by the halo, we compute the accretion-weighted specific angular momentum modulus of both components at the virial radius as

$$\langle j \rangle_{v_r} = \left| \frac{\sum_i m_i v_r \Theta(-v_r) \vec{\mathbf{r}}_i \times \vec{\mathbf{v}}_i}{\sum_i m_i v_r \Theta(-v_r)} \right|, \qquad (4)$$

where Θ is the Heaviside step function. This is done by calculating the contribution of infalling ($v_r < 0$) gas or DM particles located within the thin shell defined by $0.95 \leq r/R_{\rm vir} \leq 1.05$. Since the collisionless dark matter particles can potentially get accreted several times as they come in and out of the halo, we track each particle individually and flag them the first time they cross the virial sphere so as not to re-accrete them later. For the collisional gas, this problem does not arise as it remains in the center of the halo unless blown out/evaporated by feedback or shock-heating, so a simple radial velocity cut suffices.

Fig. 11 shows that the specific angular momenta of the accreted gas and dark matter agree reasonably well both in the NutFB and NutCO run, at all times. Although we have not included it in this paper, this turns out to be the same in the NutAD run. It is noteworthy that both freshly accreted gas and dark matter bring in a larger amount of specific angular momentum than that of the dark matter halo, $j_{\rm dm}$, which is the common assumption used in (semi-)analytic studies. The fact that $j_{\rm gas,out}$ carries nearly the same large amount of specific angular momentum as $\langle j \rangle_{v_r}$ supports the view that the angular momentum of the gas accreted by the central galaxy is acquired *before* it enters the dark matter halo.

As argued elsewhere (Pichon et al. 2011), this favours the large-scale motion of the cosmic web as the most likely origin of the angular momentum of galaxies.

The second possibility, i.e. that the amplitude of the dark matter component specific angular momentum is conserved to a lesser degree than the gas, is easily ruled out on the grounds that, as argued in Section 3.2 when the time evolution of the total specific angular momentum of *all* the baryons is calculated, it matches that of $j_{\rm dm}$ quite accurately. It seems therefore impossible to argue that dark matter loses more specific angular momentum than the gas as the main reason why $j_{\rm gas,out}$ is larger than $j_{\rm dm}$.

We are then left with the third possibility: the dissipative nature of the gas leads to a transfer of specific angular momentum distinct from that of the dark matter. As previously mentioned, cold, dense filamentary gas flows into the inner part of the dark matter halo in a dynamical time without undergoing shock-heating (e.g. Brooks et al. 2009; Powell et al. 2011). The gas subsequently settles onto the central gaseous disc, and, as a result, the outer region ($0.1 \leq r/R_{\rm vir} \leq 1$) is occupied by gas recently accreted, which has a large amount of specific angular momentum. On the other hand, dark matter particles pass through the central region of the halo and depending on their exact orbital properties, can end up populating the outer regions despite having entered the halo at earlier times with smaller angular momentum. This is shown in Fig. 12 where we plot the angular momentum as a function of position for all the DM particles belonging to the NutCO halo at z=0, colour encoding the time at which they where accreted. Whilst a lot of particles in the outer regions were accreted fairly recently (less than 5 Gyr ago), there exists a non- negligible fraction of them which were accreted at much earlier epochs (more than 7 Gyrs ago). Thus, despite the fact that dark matter first falls into the halo with a similar amount of specific angular momentum as the gas (Fig. 11), mixing with 'older' particles makes $j_{\rm dm}$ become systematically smaller than $j_{\rm gas,out}$. Note that this also explains the similar evolution of the specific angular momentum of the halo gas ($j_{\rm gas,out}$) and the newly accreted gas at high redshift (Fig. 11).

Obviously the cold, dense filamentary gas accretion disappears at low redshift (e.g. Kimm et al. 2011; Faucher-Giguère & Kereš 2011; Stewart et al. 2010), and therefore one expects that the high redshift segregation of specific angular momentum between gas and dark matter previously advocated becomes weaker as time elapses. Indeed, in the extreme case where gas is prevented from cooling (NutAD run: Fig. 2) the evolution of its specific angular momentum closely follows that of the dark matter, indicative of a similar degree of mixing of low and high specific angular momentum material for both components. However, when gas can radiatively cool, one expects this mixing process to be much less efficient as it will generally take place on timescales (typically a few sound crossing times of the halo) which are longer than the cooling time of the hot central gas. This means that the shock-heated material at the centre of the halo, which has a lower specific angular momentum than that in the outer regions, is cooled and accreted onto the central disk before it can mix with higher specific angular momentum gas. This creates a 'cooling flow' towards the central galaxy and as a result preserves the distribution of gas specific angular momentum that was set in at high redshift (Figs. 5 and 7). Note that this also explains the increasing discrepancy between dark matter and gas spin as the mass of the halo drops that we measured in large scale cosmological simulations (Section 3.4, Fig. 8): as the halos become larger, cooling timescales increase (because of higher gas temperatures and smaller central densities) allowing more and more mixing between low and high specific angular momentum gas to occur. As a result, the gap between $j_{\rm gas,out}$ and $j_{\rm dm}$ is reduced for the most massive objects.

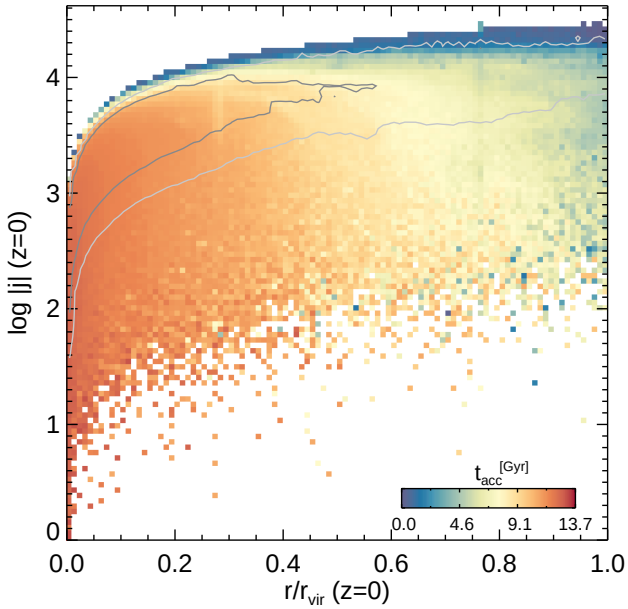

Figure 12. Distribution of angular momentum of DM particles as a function of their position for the virialised DM halo in the NutCO run at $z = 0$. Colors indicate the lookback time at which particles were accreted for the first time. Dark and light grey contours enclose 50 and 90 percent of the mass respectively. Note the large range of angular momentum values spanned by individual particles at any radius.

The redshift dependence of the spin parameter of the gas can also be understood in this framework. Again, since the cooling permits the gas to flow into the centre, $j_{\rm gas,out}$ tends to reflect j of newly accreted gas. This means that, for any dark matter halo of a given mass, its gas content at lower redshift will be composed of material carrying larger specific angular momentum. In other words, the redshift dependence of gas spin shown in Fig. 8 is understood as a large scale structure driven increase in the specific angular momentum of freshly accreted gas.

Even though we do not investigate what causes this behaviour in this paper, we remark that the systematic discrepancy between $j_{\rm dm}$ and $\langle j \rangle_{v_r}$ measured in the NutCO run at *all* times means that the dark matter component of the halo (and its baryons as a whole) loses somewhere between half and two thirds of its specific angular momentum amplitude, depending on redshift (Fig. 11). We note that even though this result seems in agreement with the measures of Book et al. (2011) for a handful of well resolved dark matter halos in pure N-body simulations, we do not find, like these authors, that it can be attributed to external torques, following the original argument of Peebles (1969). The reason for this disagreement lies in the *continuous* nature of the specific angular momentum loss of the dark matter component. As Fig. 11 demonstrates, the accretion weighted specific angular momentum of dark matter is higher than the specific angular momentum of the dark matter halo at *all redshifts*, regardless of whether we are in a phase where tidal torque theory predicts the angular momentum of the halo should grow or not. We are therefore pushed to conclude that the angular momentum 'loss' suffered by the halo has to be attributed primarily to a 'vector cancellation' effect: particles with similar amounts of angu-

lar momentum (modulus) but pointing away in opposite directions contribute only a small amount to the 'net' angular momentum of the virialised halo (e.g. Vitvitska et al. 2002). Note that the accretion history effect will also play a role in reducing the modulus of $\vec{\mathbf{j}}_{\rm dm}$ but cannot account for all the decrease.

Finally, the admittedly low spatial resolution (1–2 kpc) of the large scale cosmological hydrodynamics simulations we use to generalise our results, prevents dark matter (and gas) from forming more concentrated structures. As a result, galaxies in small halos ($N_{\rm DM} \sim 2 \times 10^3$) show a more extended disc than their NUT series counterparts. However, we believe that the properties of halos we discussed in this paper, since they are integrated over a large fraction of the halo radius, are robust. A caveat to bear in mind however, is that the physical processes that can prevent the cooling catastrophe in cluster environments are likely to change the ratio $\lambda_{\rm gas,out}/\lambda_{\rm dm}$. For example, as extensively discussed in the literature, feedback from active galactic nuclei is thought to stir/heat a large amount of cooling gas, redistributing it in the outer parts of the halo. As previously argued, such a mixing mechanism will contribute to narrow the gap between gas and dark matter spin. Such a potent feedback mechanism is not included in the cosmological simulations presented here, and thus a larger fraction of baryons than observed are converted into stars in massive haloes (Dubois et al. 2010). This should be taken into account before concluding that the ratio ($\lambda_{\rm gas,out}/\lambda_{\rm dm}$) for massive haloes has converged to ~ 2 as Fig. 8 (bottom panel) advocates.

5 CONCLUSIONS

In this paper, using high-resolution cosmological hydrodynamics re-simulations of individual galaxies and large scale cosmological hydrodynamics simulations, we have revisited the standard theory for angular momentum evolution of gas and dark matter within virialised structures.

According to this standard picture, gas acquires angular momentum through nearby tidal fields in the same way as dark matter and is shock-heated to the virial temperature during the collapse of the halo. This gas then radiatively cools and settles into a rotationally supported disc, conserving its specific angular momentum in the process (Fall & Efstathiou 1980; Dalcanton et al. 1997; Mo et al. 1998). Such assumptions naturally lead to predict that dark matter and halo gas share the same specific angular momentum. Investigating the issue, our main conclusions can be summarised as follows:

- Indeed, the time evolution of the halo gas specific angular momentum is quite comparable to that of the dark matter, but only when gas is not permitted to radiatively cool, i.e. it is artificially forced to shock- heat during the collapse (NutAD run).
- When radiative cooling is turned on, the angular momentum transport of gas becomes distinctively different from that of dark matter (NutCO run). Even though gas and dark matter still bring in a similar specific angular momentum ($\langle j \rangle_{v_r}$) when they are accreted, this amount turns out to be systematically larger than the specific angular momentum of the virialised dark matter halo as a whole ($j_{\rm dm}$) by a factor 2 to 6, depending on redshift and halo mass (see also Stewart et al. 2011).
- Regardless of whether cooling is turned on or not, the modulus of the specific angular momentum inside the virial sphere is not conserved for dark matter or gas. The amount lost ranges between one half and two thirds depending on redshift. We attribute this continuous 'loss' of angular momentum to a 'vector cancellation' effect (the angular momentum of newly accreted material is never perfectly aligned with the angular momentum of the whole halo) augmented by an accretion history effect (material accreted earlier carries less angular momentum so it weighs the average modulus of the specific angular momentum down at any epoch).
- When radiative cooling is turned on, provided one compares the dark matter with the total baryon (gas and stars) specific angular momentum, their amplitudes are similar at all times. In other words, we find no evidence of baryons losing more (or less) angular momentum than dark matter within the virialised halo at any epoch.

More specifically, our analysis reveals that at high redshift, the discrepancy between gas and dark matter specific angular momentum within $0.1 \leq r/R_{\rm vir} \leq 1.0$ ($j_{\rm gas,out}$ and $j_{\rm dm}$, respectively) arises because the angular momentum-rich freshly accreted gas flows into the central region through cold, dense filamentary accretion without being redistributed throughout the halo by shock-heating or supernovae feedback (NutFB run). As the dark matter halo grows at lower redshifts, a progressively larger amount of gas undergoes shock-heating, but since the central dense gas can still cool and collapse onto the disc on timescales shorter than a halo sound crossing time, the difference between $j_{\rm gas,out}$ and $j_{\rm dm}$ is, by and large, preserved. This competition between central cooling and redistribution of gas through shock heating and/or feedback induces a mass dependence of the discrepancy between gas and dark matter specific angular momentum: it is reduced for more massive halos where shock heating dominates. However, for a halo of fixed virial mass, this discrepancy is also larger at low redshifts than it is at high redshifts because the amount of specific momentum carried by the newly accreted material grows faster than the halo average with time (cf. Pichon et al. (2011) for the origin of this effect). This generic behaviour is encapsulated in Equation (3), which provides a fit to our simulated data.

Our efforts to probe the spatial distribution of angular momentum within the virialised halo also led us to define an inner region ($r/R_{\rm vir} \leq 0.1$). Gas in this region, $j_{\rm gas,cen}$, generally has more specific angular momentum (by a factor 2 or so) than the dark matter halo as a whole, and only stars have less (also by about a factor 2). We attribute this dichotomy within the baryon component to the long global star formation timescale of the disc compared to the gas accretion time scale, driving stars to preferentially form from gas accreted at a much earlier stage with lower angular momentum (see also Dutton & van den Bosch (2009) who reach similar conclusions with a SAM). As a result, a comparison with the data at z=0 reveals that the level of specific angular momentum of our high resolution simulated stellar disc matches quite well that of the observations. However the difficulty of obtaining realistic galaxy rotation curves still prevents us from satisfactorily reproducing the observed j versus V relation (see Fig. 10). Part of this failure is to blame on the fact that the only re-simulation we have been able to run down to z=0 so far (NutCO run) does not include any modelling of feedback (stellar winds, supernovae, cosmic ray, etc.) (as pointed out by e.g. Governato et al. 2007; Agertz et al. 2011; Brook et al. 2011). For this reason, too many baryons (the universal fraction Ω_B/Ω_m) remain in the host halo and concentrate in the galaxy, potentially affecting the morphology of our galaxy which features a large bulge (morphological type Sa/Sb) but in any case leading us to overestimate disc rotational velocities.

Overall, our results demonstrate the need for the standard picture of galaxy disc formation and evolution to undergo a major overhaul as the fundamental hypothesis upon which it is based

(specific angular momentum of the gas and dark matter within the virialised halo are the same, gas specific angular momentum is conserved) seem to be incorrect. This should have important consequences for galaxy disc sizes and therefore star formation timescales estimates used in virtually all galaxy formation models, although it is possible (albeit very unlikely) that errors induced by these two assumptions exactly cancel out. The new picture we advocate should take into account how gaseous cold flows effectively carry larger than previously thought amounts of angular momentum originating from the large-scale motion of the cosmic web down to the central region of virialised structures. The fundamental role played by gas cooling at low redshift which, for galaxy size halos, preserves this transport of angular momentum in spite of the presence of a pervasive shock-heated corona which entirely fills the virialised halo, should be described. Finally, since gas accretion at the virial radius is not perfectly aligned with the axis of rotation of the galaxy, some angular momentum will inevitably cancel out in the vicinity of the disc. Careful numerical investigation of how angular momentum is transported and/or cancelled in the central region of the halo should help shed light into this fundamental aspect of disc formation theory.

ACKNOWLEDGEMENTS

We are grateful to Romain Teyssier for insightful discussions at various stages of this work, and Amy McQuillan for a careful reading of an earlier draft of the manuscript. We thank Frank van den Bosch, Sadegh Khochfar, Leila Powell, Andrew Benson, Volker Springel, Brad Gibson, and Joel Primack for valuable comments. The NUT simulations, Cosmo25 and Cosmo50 were run on the DiRAC facility jointly funded by STFC, the Large Facilities Capital Fund of BIS and the University of Oxford. Some of the simulations in the NUT suite were also run on Jade at the CINES on resources allocated to project number GEN2191. The HORIZON-MareNostrum simulation was run at the Barcelona Supercomputing Centre. TK acknowledges support from a Clarendon DPhil studentship. JD and AS's research is supported by Adrian Beecroft, the Oxford Martin School and the STFC. CP thanks Merton College, Oxford for a visiting fellowship allowing the completion of some of this work. This research is part of the Horizon and Horizon-UK project and was also supported by an appointment to the NASA Postdoctoral Program at NASA's Goddard Space Flight Center, administered by Oak Ridge Associated Universities through a contract with NASA. YD is supported by an STFC Postdoctoral Fellowship. We also acknowledge support from the Franco-Korean PHC STAR programme.

REFERENCES

Agertz O., Teyssier R., Moore B., 2011, MNRAS, 410, 1391
Aubert D., Pichon C., Colombi S., 2004, MNRAS, 352, 376
Barnes J., Efstathiou G., 1987, ApJ, 319, 575
Bell E. F., McIntosh D. H., Katz N., Weinberg M. D., 2003, ApJS, 149, 289
Bertschinger E., 2001, ApJS, 137, 1
Bett P., Eke V., Frenk C. S., Jenkins A., Okamoto T., 2010, MNRAS, 404, 1137
Binney J., 1977, ApJ, 215, 483
Birnboim Y., Dekel A., 2003, MNRAS, 345, 349
Bond J. R., Kofman L., Pogosyan D., 1996, Nature, 380, 603
Book L. G., Brooks A., Peter A. H. G., Benson A. J., Governato F., 2011, MNRAS, 411, 1963
Bouwens R. J., Illingworth G. D., Franx M., Chary R.-R., Meurer G. R., Conselice C. J., Ford H., Giavalisco M., van Dokkum P., 2009, ApJ, 705, 936
Brook C. B., Governato F., Roškar R., Stinson G., Brooks A. M., Wadsley J., Quinn T., Gibson B. K., Snaith O., Pilkington K., House E., Pontzen A., 2011, MNRAS, pp 595–+
Brooks A. M., Governato F., Quinn T., Brook C. B., Wadsley J., 2009, ApJ, 694, 396
Bullock J. S., Dekel A., Kolatt T. S., Kravtsov A. V., Klypin A. A., Porciani C., Primack J. R., 2001, ApJ, 555, 240
Chen D. N., Jing Y. P., Yoshikaw K., 2003, ApJ, 597, 35
Cole S., Lacey C. G., Baugh C. M., Frenk C. S., 2000, MNRAS, 319, 168
Commerçon B., Hennebelle P., Audit E., Chabrier G., Teyssier R., 2008, A&A, 482, 371
Croton D. J., Springel V., White S. D. M., De Lucia G., Frenk C. S., Gao L., Jenkins A., Kauffmann G., Navarro J. F., Yoshida N., 2006, MNRAS, 365, 11
Dalcanton J. J., Spergel D. N., Summers F. J., 1997, ApJ, 482, 659
Dekel A., Birnboim Y., 2006, MNRAS, 368, 2
Dekel A., Birnboim Y., Engel G., Freundlich J., Goerdt T., Mumcuoglu M., Neistein E., Pichon C., Teyssier R., Zinger E., 2009, Nature, 457, 451
Devriendt J., Rimes C., Pichon C., Teyssier R., Le Borgne D., Aubert D., Audit E., Colombi S., Courty S., Dubois Y., Prunet S., Rasera Y., Slyz A., Tweed D., 2010, MNRAS, 403, L84
Doroshkevich A. G., 1970, Astrophysics, 6, 320
Dubois Y., Devriendt J., Slyz A., Teyssier R., 2010, MNRAS, 409, 985
Dubois Y., Teyssier R., 2008, A&A, 477, 79
Dunkley J., Spergel D. N., Komatsu E., Hinshaw G., Larson D., Nolta M. R., Odegard N., Page L., Bennett C. L., Gold B., Hill R. S., Jarosik N., Weiland J. L., Halpern M., Kogut A., Limon M., Meyer S. S., Tucker G. S., Wollack E., Wright E. L., 2009, ApJ, 701, 1804
Dutton A. A., van den Bosch F. C., 2009, MNRAS, 396, 141
Efstathiou G., Jones B. J. T., 1979, MNRAS, 186, 133
Fakhouri O., Ma C., Boylan-Kolchin M., 2010, MNRAS, 406, 2267
Fall S. M., Efstathiou G., 1980, MNRAS, 193, 189
Faucher-Giguere C., Keres D., Ma C., 2011, ArXiv e-prints
Faucher-Giguère C., Kereš D., 2011, MNRAS, pp L208+
Gottlöber S., Yepes G., 2007, ApJ, 664, 117
Governato F., Willman B., Mayer L., Brooks A., Stinson G., Valenzuela O., Wadsley J., Quinn T., 2007, MNRAS, 374, 1479
Graham A. W., Worley C. C., 2008, MNRAS, 388, 1708
Haardt F., Madau P., 1996, ApJ, 461, 20
Hahn O., Teyssier R., Carollo C. M., 2010, MNRAS, 405, 274
Hatton S., Devriendt J. E. G., Ninin S., Bouchet F. R., Guiderdoni B., Vibert D., 2003, MNRAS, 343, 75
Hoffman Y., 1986, ApJ, 301, 65
Kassin S. A., de Jong R. S., Weiner B. J., 2006, ApJ, 643, 804
Katz N., Keres D., Dave R., Weinberg D. H., 2003, in J. L. Rosenberg & M. E. Putman ed., The IGM/Galaxy Connection. The Distribution of Baryons at z=0 Vol. 281 of Astrophysics and Space Science Library, How Do Galaxies Get Their Gas?. pp 185–+
Kennicutt Jr. R. C., 1998, ApJ, 498, 541
Kereš D., Katz N., Fardal M., Davé R., Weinberg D. H., 2009, MNRAS, 395, 160
Kereš D., Katz N., Weinberg D. H., Davé R., 2005, MNRAS, 363, 2
Khochfar S., Silk J., 2011, MNRAS, 410, L42
Kimm T., Slyz A., Devriendt J., Pichon C., 2011, MNRAS, 413, L51
Mac Low M.-M., Ferrara A., 1999, ApJ, 513, 142
Maller A. H., Dekel A., Somerville R., 2002, MNRAS, 329, 423
Mo H. J., Mao S., White S. D. M., 1998, MNRAS, 295, 319
Monaco P., Fontanot F., Taffoni G., 2007, MNRAS, 375, 1189
Navarro J. F., Steinmetz M., 2000, ApJ, 538, 477
Ocvirk P., Pichon C., Teyssier R., 2008, MNRAS, 390, 1326
Peebles P. J. E., 1969, ApJ, 155, 393
Peirani S., Mohayaee R., de Freitas Pacheco J. A., 2004, MNRAS, 348, 921

Pichon C., Pogosyan D., Kimm T., Slyz A., Devriendt J., Dubois Y., 2011, ArXiv e-prints
Powell L. C., Slyz A., Devriendt J., 2011, MNRAS, pp 660–+
Prunet S., Pichon C., Aubert D., Pogosyan D., Teyssier R., Gottloeber S., 2008, ApJS, 178, 179
Rees M. J., Ostriker J. P., 1977, MNRAS, 179, 541
Sales L. V., Navarro J. F., Schaye J., Vecchia C. D., Springel V., Booth C. M., 2010, MNRAS, 409, 1541
Sharma S., Steinmetz M., 2005, ApJ, 628, 21
Silk J., 1977, ApJ, 211, 638
Somerville R. S., Hopkins P. F., Cox T. J., Robertson B. E., Hernquist L., 2008, MNRAS, 391, 481
Springel V., Hernquist L., 2003, MNRAS, 339, 289
Stewart K. R., Kaufmann T., Bullock J. S., Barton E. J., Maller A. H., Diemand J., Wadsley J., 2010, ArXiv e-prints
Stewart K. R., Kaufmann T., Bullock J. S., Barton E. J., Maller A. H., Diemand J., Wadsley J., 2011, ArXiv e-prints
Sutherland R. S., Dopita M. A., 1993, ApJS, 88, 253
Teyssier R., 2002, A&A, 385, 337
Tweed D., Devriendt J., Blaizot J., Colombi S., Slyz A., 2009, A&A, 506, 647
van de Voort F., Schaye J., Booth C. M., Haas M. R., Dalla Vecchia C., 2010, ArXiv e-prints
van den Bosch F. C., Abel T., Croft R. A. C., Hernquist L., White S. D. M., 2002, ApJ, 576, 21
Vitvitska M., Klypin A. A., Kravtsov A. V., Wechsler R. H., Primack J. R., Bullock J. S., 2002, ApJ, 581, 799
White S. D. M., 1984, ApJ, 286, 38
White S. D. M., Rees M. J., 1978, MNRAS, 183, 341
Zavala J., Okamoto T., Frenk C. S., 2008, MNRAS, 387, 364

APPENDIX: MASS ACCRETION HISTORIES

In the main body of the text, we show the time evolution of specific angular momentum for the various components of a Milky Way-like DM halo (Figs. 3 and 5). In particular, in Section 3.2, we argue that the difference in angular momentum between the central gas and the gas in the outer region of the halo arises because the mass of the central gas, which is composed of low angular momentum gas accreted at earlier time, is not negligible compared to the mass of accreting gas, and therefore reflects the history of gas accretion. To substantiate this claim, we include the mass assembly history of the various components in Fig. 13. As can be seen, the amount of gas in the central region ($M_{\rm gas} - M_{\rm gas}(r > 0.1R_{\rm vir})$) is comparable to the gas mass in the outer region ($r > 0.1R_{\rm vir}$) at all time. Thus, even if the newly accreted gas carries a larger amount of specific angular momentum, one expects that there will be a non-negligible time-delay for the entire central region to be spun at the same level. Finally, note that by multiplying Fig. 13 with Figs. 3 and 5, one can recover the total amount of angular momentum of each component.

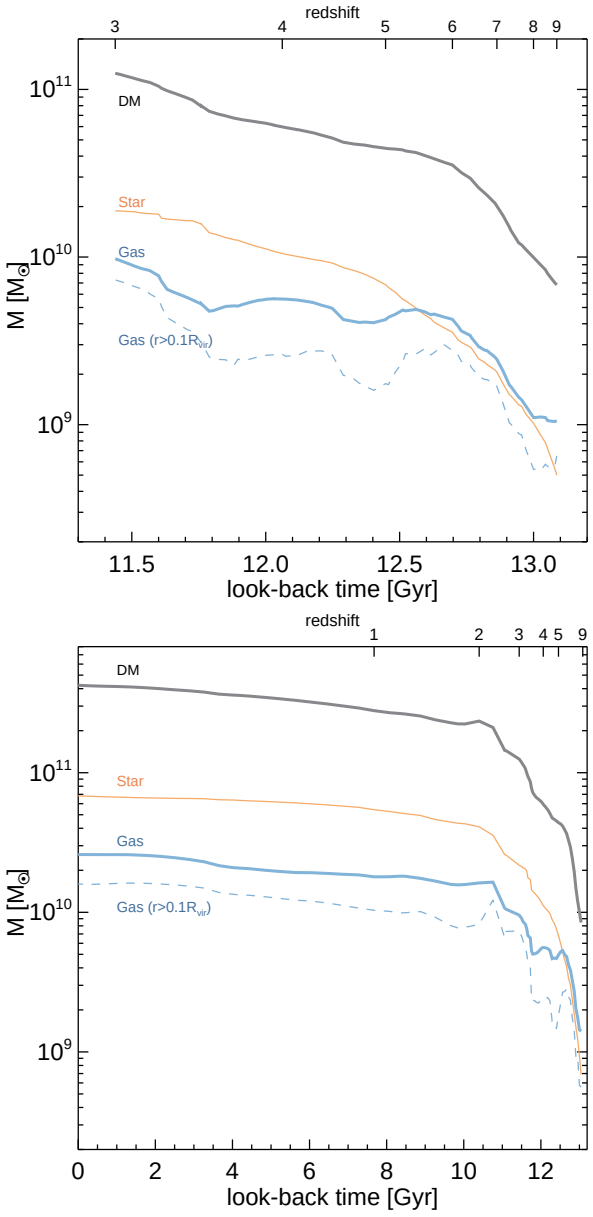

Figure 13. Mass assembly histories of the various components in the NutFB run (top) and the NutCO run (bottom). Stars, dark matter, and gas in satellite galaxies are included in the measurement. Note that the amount of gas mass in the central region ($M_{\rm gas} - M_{\rm gas}(r > 0.1R_{\rm vir})$) is comparable (a factor 2-3 lower) to the gas mass in the outer region at all times.